is a prerequisite for the complete photodegradation of organic compounds. In summary, the prevailing view[49] seems to be that the hydroxyl radical acts as the primary oxidant.

Equally convincing evidence in support of direct hole oxidation as the main step in the photooxidation process has been presented. An early study by Boonstra and Mutsaers[53] concluded that the hydroxyl radical was unlikely to participate in the reaction on TiO_2. Modification of the TiO_2 surface with chlorosilicon compounds leads to a decrease in the activity for several photocatalytic reactions, yet the effect was smaller than the extent of the eliminated hydroxyl groups. The strongest evidence for the direct hole oxidation pathway comes from a recent study[54] which failed to detect any of the expected hydroxylated intermediate OH• adducts following flash photolysis of several TiO_2/substrate combinations. We hasten to point out, however, that experimental difficulties, and the fact that OH• adducts often possess absorption bands in the UV region where TiO_2 absorption may interfere, often obstruct observations of such expected hydroxylated species.

Our results are consistent with the interpretation that adsorbed OH• (surface-trapped holes) is the major oxidant while free hydroxyl radicals play only a minor role, if any. Since we find that the OH• radical reacts with the TiO_2 at a diffusion-controlled rate, the reverse reaction, i.e., desorption of OH• to the solution, would seem unlikely. The surface-trapped hole, as defined in eq A1, could then account for most of the observations that have previously led to the suggestion of OH• radical oxidation. The formation of H_2O_2 and the observation of hydroxylated intermediates can all occur via surface reaction of this species. While we cannot entirely exclude the remote possibility that a small fraction of the OH• radicals will leak out from the "surface" and mediate the photooxidation process in the diffuse Gouy–Chapman layer, we consider this contribution to the total photooxidative process to be minimal.

Conclusions

Oxidation of small TiO_2 particles by pulse radiolytically generated OH• radicals yields trapped holes on the particle surface. The product shows a spectral maximum at $\lambda = 350$ nm. The high oxidation potential of the trapped hole is inferred from its observed decay behavior when thiocyanate is added to the TiO_2 sol. Our observations are in close agreement with the spectral features for a hole trapped on TiO_2 reported by Henglein and co-workers,[13,14] but are in clear contrast with more recent assertions.[17] The decay of the $\{TiO_2 + OH^•\}$ product follows a first-order intrinsic path (forming H_2O_2) by collapse of two trapped holes on the same particle. In the presence of adsorbed a SCN^-, the same trapped holes may oxidize the adsorbate to yield the oxidized dimer radical anion $(SCN)_2^{•-}$. From the present work, together with earlier evidence, it can be argued that photooxidation reactions occur at the semiconductor particle surface primarily via this trapped hole.

Acknowledgment. Support by the Natural Sciences and Engineering Research Council of Canada and by the Office of Basic Energy Sciences, Division of Chemical Science, US-DOE, under contract no. W-31-109-ENG-38 is gratefully acknowledged. We are grateful to Prof. J. Fendler and Ms. Youxin Yuan (Syracuse University) for their courtesy and assistance in using the light-scattering apparatus, Mr. Liao Youxin (MSD, Argonne) for his assistance with electron microscopy, and to Dr. R. Le Van Mao and Mr. B. Sarjiel (Concordia University) for BET analysis.

Registry No. TiO_2, 13463-67-7; OH•, 3352-57-6.

(50) Navio, J. A.; Rives-Arneau, V. *Langmuir* **1990**, *6*, 1525.
(51) Bickley, R. I.; Jayanty, R. K. M.; Navio, J. A.; Vishwanatham, V. In *Homogenous and Heterogenous Photocatalysis*; Nato-ASI Series C; Pelizzetti, E., Serpone, N., Eds.; D. Reidel: Dordrecht, 1986; Vol. 174, p 555.
(52) Munuera, G.; Gonzalez-Elipe, A. R.; Rives-Arneau, V.; Navio, J. A.; Malet, P.; Soria, J.; Conesa, J. C.; Sanz, J. In *Adsorption and Catalysis on Oxide Surfaces*; Che, M., Bonds, G. C., Eds.; Elsevier: Amsterdam, 1985; p 113.
(53) Boonstra, H.; Mutsaers, C. *J. Phys. Chem.* **1975**, *79*, 1940.
(54) Draper, R. B.; Fox, M. A. *Langmuir* **1990**, *6*, 1396.

Inhomogeneous Decay Kinetics and Apparent Solvent Relaxation at Low Temperatures

Richard S. Fee, John A. Milsom, and Mark Maroncelli*

Department of Chemistry, 152 Davey Laboratory, The Pennsylvania State University, University Park, Pennsylvania 16802 *(Received: December 3, 1990)*

We have observed time-dependent shifts in the fluorescence spectra of solvatochromic probe molecules in frozen polar solvents. The phenomenon is a general one and is observed in a variety of fluorophores in both hydrogen-bonding and non-hydrogen-bonding solvents. These shifts are not related to solvent relaxation but rather result from inhomogeneous fluorescence decay kinetics. Molecules in different portions of the fluorescence spectrum decay at different rates and thereby cause the spectrum to evolve in time due to nonuniform loss of excited-state population. We have modeled such kinetics based on the assumption that fluorescence decay rates are solvent sensitive only through the relation between the radiative rate and emission frequency, $k_{rad} \propto \nu^3$. Measurements of the effect of excitation wavelength on steady-state fluorescence spectra are used to quantify the inhomogeneous broadening present in a number of fluorophore/solvent systems. These results are then used as input to model their time dependence. In most cases, nearly quantitative agreement between the calculated and observed spectral dynamics is achieved.

I. Introduction

In the past few years a number of researchers have employed time-resolved fluorescence to probe the dynamics of solvation in polar solvents.[1] These measurements involve the use of solvatochromic fluorophores, probe molecules that exhibit large frequency shifts in their fluorescence spectra as a function of solvent polarity. Such probes are excited with an ultrafast laser pulse, and their subsequent fluorescence is monitored as a function of time. Time-dependent fluorescence shifts are then interpreted in terms of relaxation of the solvent environment in response to the change in solute charge distribution produced by electronic excitation.

Most current work of this type has focused on the behavior of liquids near room temperature;[2] however, we have also been pursuing such studies in low-temperature alcohols, where the dynamics appear to be qualitatively different.[3,4] During the course

(1) See for example the recent reviews: Maroncelli, M.; MacInnis, J.; Fleming, G. R. *Science* **1989**, *243*, 1674. Barbara, P. F.; Jarzeba, W. *Adv. Photochem.* **1990**, *15*, 1. Bagchi, B. *Annu. Rev. Phys. Chem.* **1990**, *40*, 115.

(2) Recent exceptions are: Barigelletti, F. *J. Phys. Chem.* **1988**, *92*, 3679. Kim, H.-B.; Kitamura, N.; Tazuke, S. *J. Phys. Chem.* **1990**, *94*, 1414. Richert, R. *Chem. Phys. Lett.* **1990**, *171*, 222.

0022-3654/91/2095-5170$02.50/0

of this latter work we have observed a curious phenomenon whose explanation forms the subject of the present report. We have found that, even at very low temperatures where solvent dynamics are expected to be unobservably slow, time-dependent spectral shifts still occur. Such shifts are a general phenomenon common to all solvatochromic probes in polar solvents. Rather than having an origin in solvent dynamics, these time-dependent shifts arise from an inhomogeneous kinetic mechanism.

The phenomenon is similar to one that has been previously observed in the myoglobin–CO system at low temperatures. Following CO photodissociation, a time-dependent blue shift of the near-IR absorption is observed. This shift has been shown to result from the presence of an inhomogeneous distribution of activation barriers to recombination.[5,6] Specifically, the distribution of barriers happens to be correlated with the absorption frequency in such a way that molecules absorbing on the red edge of the spectrum recombine faster than molecules on the blue edge. This inhomogeneous kinetics gives rise to a time-dependent spectral shift, even in the absence of any sort of relaxation process interconverting species absorbing at different wavelengths.

The fact that a similar mechanism might be operative in the time-dependent fluorescence shifts of solvatochromic probes was recently proposed by Agmon.[7] Noting an unusual nonexponentiality in the total fluorescence of coumarin 153 (Cu153) in 1-propanol,[8] he conjectured that a substantial portion of the time-dependent fluorescence shift previously attributed to solvation dynamics might instead have a nonrelaxational origin. Although further experiments and analysis[9] have shown this to be unlikely at high temperatures, in frozen solvents just such an inhomogeneous mechanism does appear to explain the observed spectral dynamics. The scenario is analogous to that discussed for the myoglobin case. In a polar solvent, solutes occur distributed among a range of local environments. For solvatochromic probes such as Cu153, the instantaneous distribution of solvent environments produces an instantaneous distribution of absorption and fluorescence frequency shifts. At sufficiently low temperatures, where different solvent environments do not interconvert during the fluorescence lifetime, the distribution can be termed inhomogeneous with respect to the fluorescence. That is, if the fluorescence lifetime varies with solvent site, the fluorescence decay will consist of a superposition of the independent decays of molecules in different environments. If, in addition, the fluorescence decay rate of a given molecule is somehow correlated with its spectral shift, inhomogeneous spectral kinetics can result. For example, assuming that blue-emitting molecules have a greater decay rate than red-emitting molecules, a time-dependent red shift of the fluorescence spectrum will occur due to a relative depletion of the blue spectral edge. A number of mechanisms might be proposed for the solvent-induced modification of the fluorescence decay rates required to produce such spectral dynamics. One simple and quite general mechanism is the fact that the radiative rate of a fluorescence transition is proportional to the cube of the emission frequency, $k_{rad} \propto \nu^3$.[10] This dependence is unrelated to solvent–solute interactions and merely results from the fact that the density of photon states varies as ν^3. However, for the probes studied here we find that the dependence $k_{rad} \propto \nu^3$ is sufficient to explain the spectral dynamics observed at low temperatures.

The outline of the remainder of the paper is as follows. Section II provides information on the fluorescent probes, solvents, and experimental methods used. In section III we describe the general features of the time-dependent spectral shifts observed in low-temperature glassy solvents and compare them to what is observed in fluid solutions at higher temperatures. Although the shifts in these two regimes are qualitatively similar, we discuss how the observed temperature dependence rules out any reasonable solvent relaxation mechanism for low-temperature spectral dynamics. In section IV, we then present the inhomogeneous kinetic model used to explain the low-temperature data. In order to model the spectral dynamics, some method for quantitating the inhomogeneity in the fluorescence spectrum is needed. Measurements of steady-state fluorescence shifts as a function of excitation wavelength, "red-edge excitation" experiments (see below), provide a means for such quantitation. In section V, we apply the model developed in section IV to analyze the red-edge excitation experiments. These results are then used to predict the time-dependent behavior of the fluorescence spectra in section VI. In most cases, nearly quantitative agreement is obtained between the spectral dynamics so predicted and the observed spectral shifts. Finally, in section VII we conclude by summarizing our major results and discussing their implications for measurements of solvation dynamics.

SCHEME I

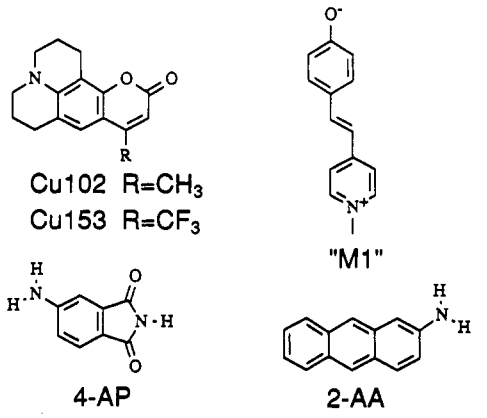

II. Experimental Section

The fluorescence probe molecules used in these studies included the coumarin dyes 102 and 153 (Cu102, Cu153), 4-aminophthalimide (4-AP), 2-aminoanthracene (2-AA), and the merocyanine dye "M1" (4-[(1-methyl-4(1*H*)-pyridinylidene)-ethylidene]-2,5-cyclohexadien-1-one), illustrated in Scheme I. The coumarin dyes (Kodak) and M1 (Aldrich) were used as received. The samples of 2-AA (Aldrich) and 4-AP (Kodak) were recrystallized several times from ethanol and methanol, respectively, prior to use.

A few comments are in order concerning the probe molecules chosen for these studies. The dyes Cu102[9,11,12] and Cu153[8,13] as well as 4-AP[14-17] have been extensively used as probes in studies of solvation dynamics. These molecules all show very large shifts in their fluorescence frequencies as a function of solvent polarity, especially in hydrogen-bonding solvents. They all have well-separated $S_0 \rightarrow S_1$ absorptions as judged by fluorescence polarization studies and quantum yields of near unity.[18] The probe

(3) Fee, R. S.; Chapman, C. F.; Maroncelli, M. Manuscript in preparation.
(4) See also: Kinoshita, S.; Nishi, N. *J. Chem. Phys.* **1988**, *89*, 6612.
(5) Campbell, B. F.; Chance, M. R.; Friedman, J. M. *Science* **1987**, *238*, 373.
(6) Agmon, N. *Biochemistry* **1988**, *27*, 3507.
(7) Agmon, N. *J. Phys. Chem.* **1990**, *94*, 2959.
(8) Maroncelli, M.; Fleming, G. R. *J. Chem. Phys.* **1987**, *86*, 6221; **1990**, *92*, 3251.
(9) Maroncelli, M.; Fee, R. S.; Chapman, C. F.; Fleming, G. R. *J. Phys. Chem.* **1991**, *95*, 1012.
(10) Birks, J. B. *Photophysics of Aromatic Molecules*; Wiley: New York, 1970; Chapter 4.
(11) Kahlow, M. A.; Kang, T. J.; Barbara, P. F. *J. Chem. Phys.* **1988**, *88*, 2372.
(12) Chapman, C. F.; Fee, R. S.; Maroncelli, M. *J. Phys. Chem.* **1990**, *94*, 4929.
(13) Jarzeba, W.; Walker, G. C.; Johnson, A. E.; Barbara, P. F. *Chem. Phys.* **1991**, *152*, 57.
(14) Ware, W. R.; Lee, S. K.; Brant, G. J.; Chow, P. P. *J. Chem. Phys.* **1971**, *54*, 4729.
(15) Mazurenko, Yu. T.; Udal'tsov, V. S. *Opt. Spectrosc. (USSR)* **1978**, *45*, 765.
(16) Yeh, S. W.; Philips, L. A.; Webb, S. P.; Buhse, L. F.; Clark, J. H. In *Ultrafast Phenomena IV*; Auston, D. H., Eisenthal, K. B., Eds.; Springer: Berlin, 1984; p 359.
(17) Nagarajan, V.; Brearley, A. M.; Kang, T. J.; Barbara, P. F. *J. Chem. Phys.* **1987**, *86*, 3183.
(18) Fee, R. S.; Maroncelli, M. Unpublished results.

2-AA has not been used in past studies of solvation dynamics, but with the exception of a smaller solvent sensitivity, it shares many of the desirable features of the former probes.[19-21] We include it here in order to demonstrate the generality of the low-temperature time-dependent shifts. Finally, M1 is not a typical fluorescence probe in that it is very weakly fluorescent in fluid solutions. For example, we have measured its quantum yield to be 0.006 in room-temperature propanol. What causes this loss of fluorescence in fluid solutions is not known; however, it is inoperative in the frozen solutions used here, where quantum yields approach unity.[18] Our interest in this molecule is due to the extreme dependence of its absorption frequency on solvent.[22] For example, there is a 125-nm blue shift in its absorption spectrum between the solvents acetone and water. Resonance Raman studies[23] have shown that this extreme solvent sensitivity is due to changes in the mixture of benzenoid/quinoid character of the ground state with solvent. Our expectation was that such unusual behavior might produce an unusually large inhomogeneity in the absorption spectrum and thus large time-dependent shifts in the fluorescence at low temperatures.[24] This did not turn out to be the case; however, data obtained with this probe are still useful for demonstrating the generality of low-temperature time-dependent shifts.

The solvents 1-propanol, ethylene glycol, and glycerol were Aldrich spectral grade, dried over molecular sieves, but otherwise used as received. Propylene carbonate (Aldrich reagent grade) was purified by vacuum distillation.

Samples for absorption and fluorescence measurements were prepared in 1-cm quartz cuvettes so as to have optical densities of ~1.0 and ~0.1, respectively, at the maximum of longest wavelength absorption band. Such optical densities correspond to concentrations of roughly 5×10^{-4} M in the absorption and 5×10^{-5} M in the fluorescence experiments. With the exception of glycerol samples, fluorescence samples were deoxygenated by N_2 bubbling and then vacuum-sealed with a removable Teflon fitting. (Glycerol samples were not deoxygenated.) For low-temperature measurements, sealed cuvettes were enclosed in a copper block mounted on the cold finger of an APD liquid N_2 cryostat. With this system, temperatures between 85 and 300 K could be maintained constant to within ±2 K for the many hours needed for the red-edge and time-resolved experiments.

Steady-state absorption and emission spectra were recorded with Perkin-Elmer Lambda 6 and Spex Fluorolog F212 spectrometers. In most cases instrumental parameters were chosen to provide resolutions of 1 and ~2 nm in absorption and emission, respectively. Further reductions in resolution had a negligible effect on the spectra even at the lowest temperatures studied. Fluorescence spectra were corrected for instrumental response, and both absorption and fluorescence spectra were converted from a linear wavelength to a linear frequency representation prior to analysis. Quantum yields were measured relative to a quinine sulfate/1.0 N H_2SO_4 standard, whose yield was taken to be 0.546 with 360-nm excitation.[25]

Time-resolved spectra were measured by use of a time-correlated single-photon counting system having an overall instrumental response time of 50 ps (fwhm).[12] Emission was collected through a $^1/_4$-m monochromator (ISA H-10) having a band-pass of 4 nm. Spectra were reconstructed from a series of ~15 fluorescence decays at selected emission wavelengths in the manner described in detail in refs 8 and 12. Briefly, the decays were fit to a sum-of-exponentials form by using an iterative reconvolution scheme in order to partially remove the effects of instrumental broadening.

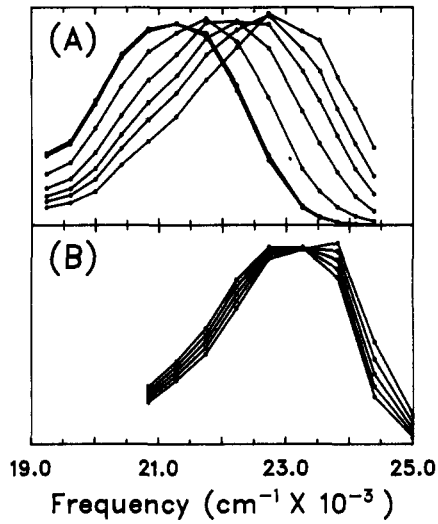

Figure 1. Time-resolved fluorescence spectra of Cu102 in 1-propanol. Spectra have been normalized to constant height. (A) T = 253 K; the spectra correspond to times of 0, 25, 50, 100, 250, 1000, and 10000 ps, from right to left. (B) T = 85 K; the spectra correspond to times of 0, 2, 4, 6, and 8 fluorescence lifetimes (τ_{fl} = 3.65 ns) from right to left. The apparent isoemissive point in these spectra is only coincidental; log-normal fits to these data do not exhibit such a stationary point.

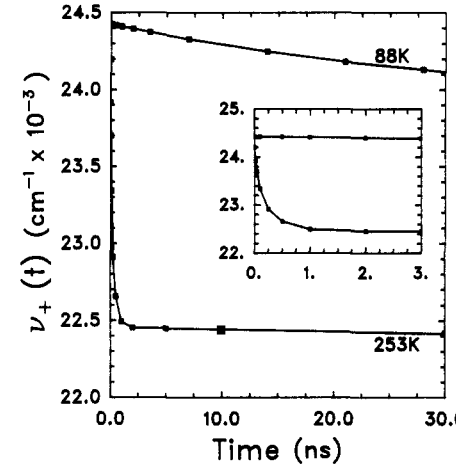

Figure 2. Time evolution of the fluorescence frequency, $\nu_+(t)$ derived from the spectra shown in Figure 1 (Cu102/1-propanol). ν_+ is defined as the frequency of the half-height point on the high-frequency side of the spectrum. The inset shows the same data on an expanded scale.

The set of fitted decays were then relatively normalized by comparing the time-integrated intensity obtained at a given emission wavelength to the corresponding intensity in the steady-state fluorescence spectrum. To extract measures of the frequency change with time, the spectra at any given time were usually fit to a log-normal line shape as discussed in ref 8.

III. Low-Temperature Shifts

General features of the time-dependent spectral shifts we have observed with a variety of probe/solvent combinations are illustrated by the Cu102/propanol data shown in Figures 1 and 2. Figure 1 compares time-evolving fluorescence spectra recorded at 253 and 88 K. Characteristic frequencies of these spectra are plotted as a function of time in Figure 2.

At sufficiently high temperatures, the fluorescence of Cu102 in propanol exhibits a large time-dependent red shift, which is essentially complete within its fluorescence lifetime (Figure 1A). Probes such as Cu102 are utilized in solvation studies because the magnitude of their time- or solvent-dependent shift is comparable to their spectral width. In the present example, the shift is ~1500 cm^{-1}, compared to a width of ~2900 cm^{-1} (fwhm). The shift takes place with an average time constant of 210 ps at 253 K, compared to a fluorescence lifetime of ~5 ns at this tem-

(19) Rotkiewicz, K.; Grabowski, Z. R. *Trans. Faraday Soc.* **1969**, *65*, 3263.
(20) Schulman, P. G.; Kovi, P. J.; Torosian, G.; McVeigh, H.; Carter, D. *J. Pharm. Sci.* **1973**, *62*, 1823.
(21) Abdullah, K. A.; Kemp, T. J. *J. Photochem.* **1985**, *30*, 363.
(22) Jacques, P. *J. Phys. Chem.* **1986**, *90*, 5535 and references therein.
(23) Tsukada, M.; Mineo, Y.; Itoh, K. *J. Phys. Chem.* **1989**, *93*, 7989.
(24) Red-edge excitation experiments of the sort carried out here were also performed on the M1 probe by Al-Hassan et al. (Al-Hassan, K. A.; El-Bayoumi, M. A. *Chem. Phys. Lett.* **1980**, *76*, 121).
(25) Demas, J. N.; Crosby, G. A. *J. Phys. Chem.* **1971**, *75*, 991.

TABLE I: Solvent Dependence of the Fluorescence Properties of Cu102 (20 °C)

solvent	n^{20}_D[a]	τ_{fl},[b] ns	ϕ_{fl}[c]	k_{rad},[d] ns^{-1}	k_{nr},[e] ns^{-1}	$10^3\langle\nu\rangle$,[f] cm^{-1}	$10^{12}\langle\nu^3\rangle$,[f] cm^{-1}
1. cyclohexane	1.463	2.99	0.80	0.28	0.057	24.0	5.71
2. triethylamine	1.410	2.66	0.57	0.22	0.16	23.6	5.48
3. diethyl ether	1.352	3.14	0.82	0.26	0.059	23.2	5.32
4. *n*-butyl acetate	1.394	3.13	0.77	0.25	0.073	22.6	5.06
5. tetrahydrofuran	1.407	3.54	0.87	0.25	0.036	22.5	5.00
6. acetone	1.359	4.08	0.78	0.19	0.053	21.7	4.62
7. dimethylformamide	1.430	3.97	0.82	0.21	0.052	21.4	4.53
8. propylene carbonate	1.419	4.30	0.86	0.20	0.033	21.3	4.50
9. dimethyl sulfoxide	1.479	3.88	0.89	0.23	0.027	21.2	4.43
10. 1-propanol	1.386	4.53	0.79	0.17	0.046	20.9	4.30
11. methanol	1.328	5.01	0.81	0.16	0.037	20.5	4.14

[a] Solvent refractive index, from: Riddick, J. A.; Bunger, W. B.; Sakano, T. K. *Organic Solvents*: Wiley: New York, 1986. [b] Fluorescence lifetime, ±5%. [c] Fluorescence quantum yield, ±10%. [d] Radiative rate constant, $k_{rad} = \phi_{fl}/\tau_{fl}$. [e] Nonradiative rate constant, $k_{nr} = (1 - \phi_{fl})/\tau_{fl}$. [f] Average frequencies of the fluorescence spectrum ($F(\nu)$) defined by $\langle\nu\rangle = \int F(\nu)\nu\, d\nu / \int F(\nu)\, d\nu$ and $\langle\nu^3\rangle = \int F(\nu)\, d\nu / \int F(\nu)\nu^{-3}\, d\nu$.

TABLE II: Results of Red-Edge Excitation and Time-Resolved Fluorescence Experiments

		spectral characteristics[b]		red-edge results[c]		spectral dynamics[d]			
probe	solvent/T[a]	$10^3\Delta\Delta\nu$, cm^{-1}	$10^3\Gamma_{abs}$, cm^{-1}	$10^3\Gamma_{inh}$, cm^{-1}	$10^3\nu_{00}$, cm^{-1}	τ_{fl}, ns	$(d\nu/dt)_{obs}$, cm^{-1} ns^{-1}	$(1/k_{fl})(d\nu_+/dt)_{obs}$, cm^{-1}	$(1/k_{rad})(d\nu_+/dt)_{calc}$, cm^{-1}
1. Cu153	1-PrOH/88 K	2.2	3.6	1.3 ● 0.2	22.0	5.12	8.8	45	56
2. Cu102	1-PrOH/85 K	2.0	3.1	0.79 ± 0.05	24.10	3.60	9.9	36	15
3. M1	1-PrOH/85 K	1.0	2.7	1.0 ± 0.1	19.91				
4. 2-AA	1-PrOH/86 K	1.1	3.6	0.9 ● 0.1	22.6	23.9	1.0	24	19
5. 4-AP	1-PrOH/88 K	3.4	4.1	1.3 ± 0.1	23.56	18.4	1.9	35	39
6. 4-AP	glycerol/160 K	3.5	4.5	1.8 ● 0.1	23.32	17.9	5.6	100	87
7. 4-AP	glycerol/92 K	3.5	4.6	2.0 ± 0.2	23.28	18.3	3.3	60	83
8. M1	4:1 EG:H_2O/86 K	1.6	3.4	1.3 ● 0.2	20.62	2.20	15	33	53
9. Cu102	PC/86 K	1.4	3.4	1.2 ● 0.2	24.28	3.40	7.1	24	21

[a] 1-PrOH = 1-propanol, EG = ethylene glycol, and PC = propylene carbonate. The solvent for experiment 8 was a 4:1 volume ratio mixture of ethylene glycol and water. [b] $\Delta\Delta\nu$ is the difference between the Stokes shifts ($\nu_{abs} - \nu_{em}$) observed at 298 and 88 K. This parameter measures the extent of frequency shift in fluorescence that is available through solvent reorganization. Γ_{abs} is the full width at half-maximum of the absorption spectrum (at the indicated temperature). [c] Parameters derived from the analysis of red-edge excitation experiments. Γ_{inh} is the width (fwhm = (8 ln 2)$^{1/2}\sigma$) of the $p(\delta)$ distribution. ν_{00} is the inversion frequency defined in eq 5, which corresponds to the electronic origin. [d] τ_{fl} is the time constant for loss of the total (wavelength-integrated) fluorescence. $(d\nu_+/dt)_{obs}$ is the observed slope of the $\nu_+(t)$ curves measured from time-resolved fluorescence spectra. $(1/k_{fl})(d\nu_+/dt)_{obs}$ is the slope normalized with respect to the total fluorescence decay rate. $(1/k_{rad})(d\nu_+/dt)_{calc}$ is the corresponding normalized slope calculated on the basis of the inhomogeneous decay model. Comparison of these two parameters relies on the assumption that $k_{rad} \cong k_{fl}$, i.e., that $k_{nr} \ll k_{rad}$.

perature. Small changes in width do occur; however, the dynamics are reasonably well described in terms of a spectrum of fixed shape whose frequency varies continuously in time. This shift is usually interpreted as reflecting the dynamical solvent reorganization that takes place after probe excitation.[1,11-17]

At low temperatures, and in particular at temperatures where one would expect solvent relaxation to be frozen out, we observe qualitatively similar spectral dynamics. The spectra of Cu102 recorded in propanol glass at 88 K (Figure 1B) are representative. Here again we observe a continuous shift of the spectrum with little apparent change in its shape or width. (The apparent isoemissive point in this series of low-resolution spectra is only coincidental.) The shifts are much smaller during the fluorescence lifetime of the probe. Typically the observable shift amounts to ~10% of that observed at high temperatures. But, apart from the large difference in rate, there is little that distinguishes between the spectral changes observed at high and low temperatures. It might therefore be reasonable to ascribe these low-temperature shifts to residual solvent dynamics occurring in low-temperature glassy solvents.

However, several observations serve to refute this possibility. First, the apparent solvent dynamics depend markedly on probe molecule considered. For example, there is a 10-fold difference in the rate of spectral shift among the probes studied in propanol at 88 K (Table II). Such behavior is contrary to the nearly probe-independent solvation times measured at higher temperatures.[1] Second, experience with alcohols at higher temperatures[3,8] shows that average solvation times at such low temperatures should be much greater than the fluorescence lifetime. For example, at 164 K solvation times in 1-propanol are roughly 20 ns and show an Arrhenius temperature dependence (over the range 150–250 K) with activation energy of 19 kJ/mol.[3] On the basis of this high-temperature trend, one would predict a solvation time of ~3 ms at 88 K! Furthermore, the spectral shifts observed at low temperatures do not exhibit activation energies consistent with any reasonable type of solvent relaxation. An extreme example is provided by results obtained with 4-AP iin glycerol (Table II). At 160 K, glycerol is already a glass (T_g = 190 K[26]) and solvent dynamics should be frozen out on the fluorescence time scale. At this temperature we observe small time-dependent spectral shifts of the same sort illustrated in Figure 1b. Lowering the temperature by more than a factor of 2, to 90 K, causes less than a factor of 2 change in the rate of spectral shift. (This change is related to differences in spectral inhomogeneity discussed below.) Clearly, no normal solvent relaxation could be responsible for such activationless behavior. Rather, these low-temperature shifts have a purely nondynamical origin, and they can be quantitatively understood in terms of an inhomogeneous kinetic model described in the next section.

IV. Inhomogeneous Kinetic Model

The model we use to interpret the time-dependent shifts observed at low temperatures involves two ingredients. The first is a rather standard picture[27] of solvent-induced spectral broadening in the static limit. Probe molecules are envisioned to be distributed among a range of different local solvent environments. Solute–solvent interactions vary with environment, and these variations modulate the ground- and excited-state energies and give rise to shifts in the probe spectrum as a function of site. The

(26) Angell, C. A.; Sare, J. M.; Sare, E. J. *J. Phys. Chem.* **1978**, *82*, 2622.
(27) For example, ref 4 considers the effect of a distribution of solvent environments on electronic spectra using a model whose essential ingredients are the same as those employed here.

solvent is assumed to be frozen on the time scales of interest so that the effect of this environmental distribution is an inhomogeneous broadening of both the absorption and emission spectra. The second ingredient required for observing time-dependent fluorescence shifts is a fluorescence decay rate that varies systematically with the solvent-induced spectral shift. Such a solvent-dependent decay rate can arise from a number of effects. Here we attribute the dependence to the fact that radiative rates vary with emission frequency, independent of solvent–solute interactions.

We now consider quantitative implementation of these ideas, beginning with the spectral model. We assume that the effect of solvent environment on the probe absorption spectrum is only an overall shift by an amount δ. That is, we assume that there is a single line-shape function $g(\nu)$ that, to within a site-dependent shift, describes the absorption spectrum of all solute molecules. This function accounts for the underlying vibronic structure as well as any homogeneous broadening of the spectrum. The inhomogeneously broadened absorption spectrum, $A(\nu)$, is then given by

$$A(\nu) = c\nu \int g(\nu-\delta)\, p(\delta)\, d\delta \qquad (1)$$

In this expression, c is a constant independent of solvent site and $p(\delta)$ describes the equilibrium distribution of ground-state solutes among sites, catalogued according to spectral shift δ. The factor of ν appears in eq 1 in order to make $g(\nu)$ directly proportional to the Einstein B coefficient. For the distribution $p(\delta)$ we choose a Gaussian function:

$$p(\delta) = (2\pi\sigma^2)^{-1/2} \exp(-\delta^2/2\sigma^2) \qquad (2)$$

Such a distribution of solvent shifts follows from an equilibrium distribution of ground-state solvation energies that is Gaussian in form. Such a distribution is usually assumed[4,28,29] and observed[30-34] to be appropriate in models of polar solvation.

The fluorescence spectrum depends on how the $p(\delta)$ distribution is transferred to the excited state via the process of absorption. For a delta-function excitation at $t = 0$, the time-dependent distribution of excited states among solvent sites, δ, is given by

$$p_e(\delta,t;\nu_{exc}) = c'\nu_{exc} g(\nu_{exc}-\delta)\, p(\delta) \exp[-k(\delta)t] \qquad (3)$$

Here ν_{exc} is the excitation frequency, assumed monochromatic, c' is a proportionality constant, and $k(\delta)$ is the excited-state decay rate (total fluorescence decay rate), which is a function of solvent shift δ. Implicit in eq 3 is the assumption of a frozen solvent; time-dependent changes in the excited-state distribution in our model are due only to loss of excited-state molecules. The fluorescence spectrum at any time after excitation at frequency ν_{exc} is then given by

$$F(\nu,t;\nu_{exc}) = c''\nu^3 \int p_e(\delta,t;\nu_{exc})\, f(\nu-\delta)\, k_{rad}(\delta)\, d\delta \qquad (4)$$

where $f(\nu)$ is a fluorescence line-shape function, analogous to $g(\nu)$, and k_{rad} is the radiative rate. For simplicity we assume that the absorption and fluorescence line-shape functions obey a mirror symmetry relation of the form[10,35]

$$f(\nu) = g(2\nu_{00} - \nu) \qquad (5)$$

with ν_{00} being the electronic origin. Such a relationship requires that a single excited state be involved in the electronic transition under consideration and that the vibrational spacing in the ground and excited states be nearly equal. Both of these conditions appear to be satisfied in a number of the probes described in section II. Given this last assumption, the fluorescence spectrum at any time can be written

$$F(\nu,t;\nu_{exc}) = C\nu^3\nu_{exc} \int g(\nu_{exc}-\delta)\, p(\delta)\, g(2\nu_{00}-\nu+\delta) \times \exp\{-[k_{rad}(\delta) + k_{nr}(\delta)]t\} k_{rad}(\delta)\, d\delta \qquad (6)$$

In writing eq 6 we have explicitly decomposed the total fluorescence decay rate into radiative and nonradiative parts

$$k_{fl}(\delta) = k_{rad}(\delta) + k_{nr}(\delta) \qquad (7)$$

in order to display the slightly different influence of these two components. Finally, the steady-state fluorescence spectrum, $F_\infty(\nu)$, is obtained from the time integral of eq 6:

$$F_\infty(\nu;\nu_{exc}) = C\nu^3\nu_{exc} \int g(\nu_{exc}-\delta)\, p(\delta)\, g(2\nu_{00}-\nu+\delta)\{k_{rad}(\delta)/k_{fl}(\delta)\}\, d\delta \qquad (8)$$

To complete the model, we need an explicit representation of how the radiative and nonradiative decay rates vary with solvent shift. We have found the following approximations sufficient to explain the time-dependent shifts observed with most probe/solvent combinations studied:

$$k_{nr}(\delta) = k_{nr} \qquad (9a)$$

$$k_{rad}(\delta) \propto \langle \nu(\delta)^3 \rangle \qquad (9b)$$

In these equations $\langle \nu(\delta)^3 \rangle$ is the average cubed frequency of the site-selected fluorescence spectrum, defined by

$$\langle \nu(\delta)^3 \rangle \equiv \int f(\nu-\delta)\nu^3\, d\nu \Big/ \int f(\nu)\, d\nu \qquad (10)$$

where $f(\nu) = g(2\nu_{00}-\nu)$ is the fluorescence line shape discussed above. The first assumption, that k_{nr} is independent of δ, is a reasonable first approximation. With the probes studied here, k_{nr} does vary with solvent at room temperature (e.g., see Table I). However, with the exception of M1, differences in k_{nr} are small even at room temperature and would be expected to be of little consequence in low-temperature glasses where $k_{nr} \ll k_{rad}$. We thus assume that all of the dependence upon δ comes from the radiative component of the total decay, k_{rad}. We further assume that k_{rad} depends on solvent state only via the well-known ν^3 factor in the Einstein A coefficient.[10] This $k_{rad} \propto \langle \nu^3 \rangle$ dependence is related to the density of photon states and has no direct relationship to solvent–solute interactions. The latter may also influence the frequency dependence of k_{rad} but are not considered in the present treatment (see also section VII).

We have verified the approximate proportionality between k_{rad} and $\langle \nu^3 \rangle$ for one of the probes used in this study, Cu102. To do so we measured k_{rad} and k_{nr} in solvents for which interconversion

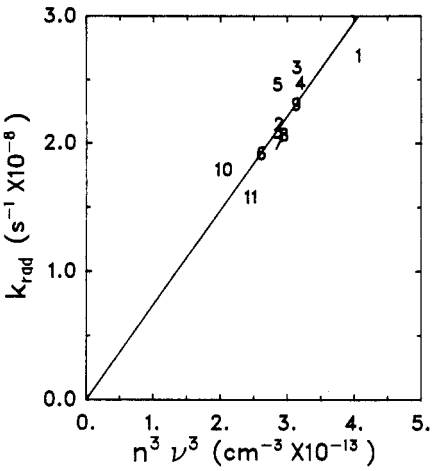

Figure 3. Radiative rates of Cu102 in different solvents, plotted as a function of $n^3\nu^3$. The numbers correspond to the solvents listed in Table I. n is the solvent refractive index, and ν^3 is the average cubed frequency defined by eq 12.

(28) Marcus, R. A. *J. Chem. Phys.* **1965**, *43*, 1261.
(29) Loring, R. F.; Yan, Y. Y.; Mukamel, S. *Chem. Phys. Lett.* **1987**, *135*, 23.
(30) Loring, R. F. *J. Phys. Chem.* **1990**, *94*, 513.
(31) Kuharski, R. A.; Bader, J. S.; Chandler, D.; Sprik, M.; Klein, M. L.; Impey, R. W. *J. Chem. Phys.* **1988**, *89*, 3248.
(32) Yoshimori, A.; Kakitani, T.; Enomoto, Y.; Mataga, N. *J. Phys. Chem.* **1989**, *93*, 8316. Hatano, Y.; Saito, M.; Kakitani, T.; Mataga, N. *Ibid.* **1988**, *92*, 1008.
(33) Carter, E. A.; Hynes, J. T. *J. Phys. Chem.* **1989**, *93*, 2184.
(34) Maroncelli, M. *J. Chem. Phys.* **1991**, *94*, 2084.
(35) Birks, J. B.; Dyson, D. J. *Proc. R. Soc. London* **1963**, *A275*, 135.

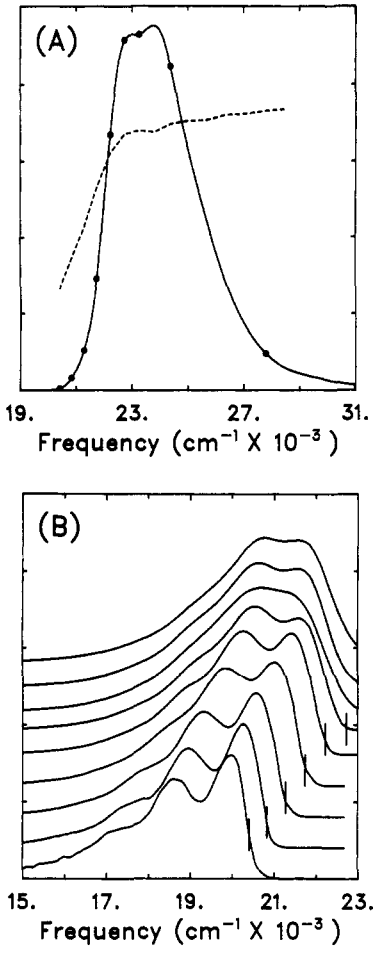

Figure 4. Red-edge excitation data for Cu153 in 1-propanol at 88 K. (A) Absorption spectrum. The points marked on the spectrum show the excitation frequencies (ν_{exc}) used to record the spectra in panel b. The dashed curve is the variation of ν_+ with ν_{exc}. (The vertical axis has been omitted here for the sake of clarity; see Figure 6.) (B) Fluorescence spectra recorded with different excitation frequencies (shown by the vertical bars on the spectra).

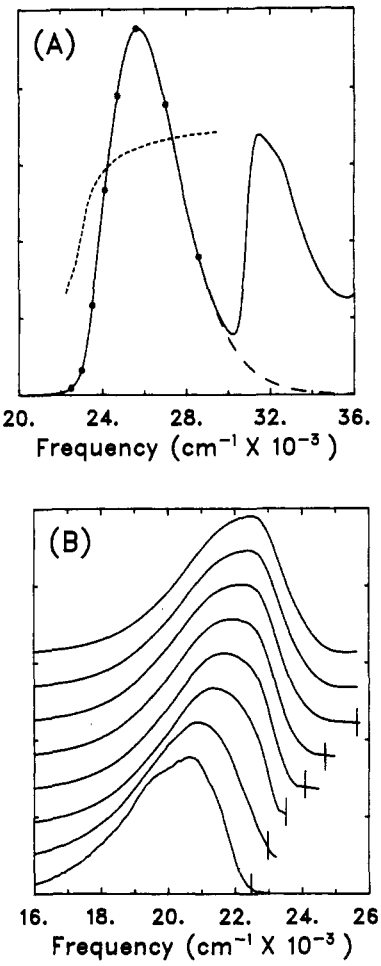

Figure 5. Red-edge excitation data for 4-AP in 1-propanol at 88 K. (A) Absorption spectrum. The points marked on the spectrum show the excitation frequencies (ν_{exc}) used to record the spectra in panel b. The dashed curve is the variation of ν_+ with ν_{exc}. (The vertical axis has been omitted here for the sake of clarity; see Figure 6.) Also shown (long dashed curve) is the fit of the high-frequency tail of the absorption spectrum used in later analysis). (B) Fluorescence spectra recorded with different excitation frequencies (shown by the vertical bars on the spectra).

among different solvent environments is much faster than k_{rad}. Results of these measurements are listed in Table I and plotted in Figure 3. If the ν^3 effect dominates the radiative rate dependence on solvent we would expect to observe[36] the relationship

$$k_{rad} \propto n^3\langle\nu^3\rangle \tag{11}$$

with the average fluorescence frequency defined by

$$\langle\nu^3\rangle \equiv \int F_\infty(\nu)\,d\nu / F_\infty(\nu)\nu^{-3}\,d\nu \tag{12}$$

In eq 11, n is the average index of refraction of the solvent at the fluorescence frequency, for which we use n^{20}_D. Figure 3 demonstrates that eq 11 (solid line) is reasonably well satisfied in the case of Cu102. Fits of this data to the relation $k_{rad}/n^3 = c\langle\nu\rangle^\alpha$ yield a power of $\alpha = 2.2 \pm 0.6$, close to the expected result (see also section VII).

V. "Red-Edge Excitation" Experiments

In order to apply the above model to predict time-dependent spectral shifts, it is necessary to determine the degree of inhomogeneity in the spectrum. That is, we must know $p(\delta)$, or since we are assuming a Gaussian function, we must know the width (σ) of this solvent-induced spectral shift distribution. We determine this width using a well-known phenomenon that we will refer to as the "red-edge excitation" (REE) effect.[24,37-44] As is clear from eq 8, for nonzero σ, the steady-state fluorescence spectrum $F_\infty(\nu)$ depends on excitation frequency. Especially for excitation on the red edge of the absorption spectrum (where $g(\nu)$ is usually sharp), the fluorescence spectrum shifts to the red as ν_{exc} is decreased. Figures 4 and 5 illustrate data obtained with the probes Cu153 and 4-AP in 1-propanol at 88 K. In each case, panel A is the absorption spectrum and panel B shows steady-state

(36) The apparent difference in the definitions of average cubed emission frequency given in eqs 10 and 12 is due to the distinction between the fluorescence spectrum $F(\nu)$ and the fluorescence line-shape function employed in the two cases. $F(\nu)$ is the observed spectrum whereas the line shape $f(\nu)$, like $g(\nu)$, is defined to be directly proportional to the Einstein B coefficient (for emission). For no solvent broadening $F(\nu) = \nu^3 f(\nu)$. For other examples of the sort of behavior described by eqs 11 and 12 see: Meech, S. R.; Phillips, D.; Lee, A. G. *Chem. Phys.* **1983**, *80*, 317.

(37) Various names have been used to label this phenomenon in the literature. For example, refs 39 use the "bathochromic shift", refs 40, 41, and 43 the "red-edge excitation" (REE), and ref 44 the "fluorescence line-narrowing" effect.

(38) Galley, W. C.; Purkey, R. M. *Proc. Natl. Acad. Sci. U.S.A.* **1970**, *67*, 1116.

(39) Rubinov, A. N.; Tomin, V. I. *Opt. Spektrosk.* **1970**, *29*, 578; **1971**, *30*, 461.

(40) Pavlovich, V. S.; Pikulik, L. G. *Zh. Prikl. Spektrosk.* **1972**, *16*, 753. Pavlovich, V. S. *Ibid.* **1975**, *25*, 1141.

(41) Itoh, K.; Azumi, T. *J. Chem. Phys.* **1975**, *62*, 3431. Azumi, T.; Itoh, K.; Shiraishi, H. *Ibid.* **1976**, *65*, 2550.

(42) Funfschilling, J.; Zschokke-Granacher, I.; Williams, D. F. *J. Chem. Phys.* **1981**, *75*, 3669.

(43) Demchenko, A. P. *Biophys. Chem.* **1982**, *15*, 101.

(44) The term "fluorescence line narrowing" is usually reserved for experiments performed at temperatures near 4 K. For a review of such experiments see: Personov, R. I. In *Spectroscopy and Excitation Dynamics of Condensed Molecular Systems*; Agranovich, V. M., Ed.; North-Holland: Amsterdam, 1983; p 555.

fluorescence spectra recorded at the different excitation frequencies marked on the absorption spectrum. Superimposed on the absorption spectra we also show the dependence of the fluorescence frequency on excitation frequency (see below). These data are typical. The most obvious changes in fluorescence occur for excitation frequencies on the red edge of the absorption spectrum. In addition to the frequency shift, the fluorescence spectrum becomes progressively more structured with decreasing ν_{exc}. Qualitatively, this movement and the development of fine structure result from the fact that red-edge excitation selects out a narrowed and frequency-dependent subset of the full solvent distribution $p(\delta)$ (eq 3). Spectral data similar to those displayed in Figures 4 and 5 have been observed and correctly interpreted in terms of solvent inhomogeneity for some time.[38,39] Curiously, we are aware of only one previous study[42] that has analyzed this effect in order to quantitatively measure the inhomogeneous broadening present in fluorescence spectra.

In order to find $p(\delta)$ from spectral data of the sort shown in Figures 4 and 5, one must know the intrinsic line-shape function $g(\nu)$. This function is not directly observable[45] but must be derived from the data in an iterative fashion. Toward this end a series of pairs $\{g_\sigma(\nu),p_\sigma(\delta)\}$ with different values of the solvent width σ are constructed. These pairs must be such that when convoluted according to eq 1 they reproduce the observed absorption spectrum. The correct σ and thus $g(\nu)$ and $p(\delta)$ are then chosen from this series as the pair that best reproduces the observed excitation dependence of the fluorescence spectrum. In practice, considerable effort is often needed to generate a series of $\{g_\sigma(\nu),p_\sigma(\delta)\}$ pairs over the range of σ required. Different approaches are necessary depending on the nature of the spectra involved. The most direct method is to simply take the absorption spectrum $(A(\nu)/\nu)$ and, after removing interfering bands (see for example Figure 5A), numerically deconvolute from it a Gaussian of width σ.[46] Numerical deconvolution assures that the absorption spectrum is exactly reproduced and requires no prior assumptions concerning the shape of $g(\nu)$. This method worked well for most of the 4-AP spectra studied (for example that shown in Figure 7B). Unfortunately, when the width of the solvent shift distribution is greater than ~30% of the width of the absorption spectrum, the deconvolution procedure becomes numerically unstable. When such cases arise, some other method for guessing $g(\nu)$ must be employed. Both deconvolution of suitably shifted and inverted red-edge fluorescence spectra, and synthesis of $g(\nu)$ based on a sum of displaced harmonic oscillators model,[47-49] were used when necessary. The more structured spectra of Cu153 (Figure 7A) represented one case where such methods were needed. Although the latter decomposition methods are not uniquely prescribed, it is sufficient that the $g(\nu)$ so obtained reproduce the absorption spectrum upon convolution with $p(\delta)$. With some effort this end could be achieved in all cases studied here.

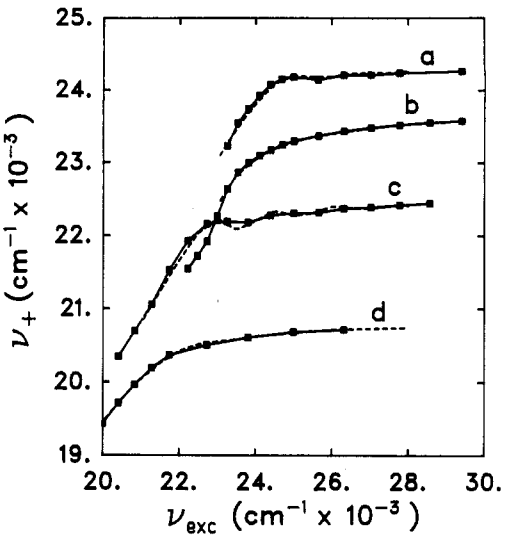

Figure 6. Dependence of emission frequency ν_+ on excitation frequency for some representative probe/solvent combinations. In each case the points and solid curve denote experimental data and the dashed curve is the fit to the model described in the text. All temperatures are ~88 K (see Table II), and the solvent is 1-propanol unless otherwise noted. The systems shown are (a) Cu102, (b) 4-AP, (c) Cu153, and (d) M1 in a 4:1 ethylene glycol/water mixture. Values of the model parameters ν_{00} and $\sigma(\Gamma_{inh})$ used to achieve these fits are listed in Table II.

After generating an appropriate set of $\{g_\sigma(\nu),p_\sigma(\nu)\}$ pairs, the correct solvent width σ must be chosen. The first test for correct σ is prediction of the fluorescence frequency shift as a function of excitation frequency. As a measure of fluorescence frequency, we choose the half-height point on the high-frequency edge of the fluorescence spectrum, which we denote ν_+. This point is sharply defined due to the steepness of the blue edge of the fluorescence spectrum, and its use avoids problems associated with measuring the peak position in a partially structured spectrum. The observed dependence of ν_+ on ν_{exc} is shown superimposed on the absorption spectra of Figures 4 and 5. These curves are also reproduced in Figure 6 along with representative experimental data obtained in two other systems (solid curves). The dashed curves in Figure 6 were obtained from spectra calculated on the basis of eq 8 with optimized values of σ (and ν_{00}). Fitting parameters are listed in Table II. As can be seen from Figure 6, good agreement can be achieved on the basis of the simple model described in section IV. The form of the $\nu_+(\nu_{exc})$ curves are sensitive to the shape of the absorption spectra and show oscillations where $g(\nu)$ is structured. Even these oscillations are reasonably reproduced by the calculated curves, with small residual deviations being the result of inaccuracies in the $g(\nu)$ function.

Two examples of spectral decompositions determined by such fits to the red-edge frequency shifts are shown in Figure 7. In both examples (1-propanol, 88 K) the best fit was achieved for a solvent shift distribution having a full width of 1300 cm^{-1} (fwhm, listed as Γ_{inh} in Table II; $\Gamma_{inh} = (8 \ln 2)^{1/2}\sigma$). This inhomogeneous solvent broadening is substantial, amounting to 30–40% of the overall vibronic width of these probes. At the lowest temperatures accessible here, 86 K, the intrinsic line shapes are still broad and, except for Cu153 (Figure 7A), relatively structureless. This implies that there is also a substantial homogeneous broadening operating at this temperature. For example, the substructure in the $g(\nu)$ determined for Cu153 exhibits line widths of ~700 cm^{-1}. If we assume that this number corresponds to the line width of a single vibronic transition, the dephasing time implied would be ~7 fs. Since recent femtosecond studies[50-52] show dephasing times

(45) At much lower temperatures ($T \sim 4$ K), where the homogeneous spectral width is much smaller than the width of $p(\delta)$, monochromatic excitation near ν_{00} selects out what is virtually a delta-function solvent distribution. In this case the narrowed fluorescence spectrum can be a nearly direct representation of the intrinsic line-shape function $g(\nu)$ (actually $\nu^3 g(2\nu_{00} - \nu)$). (See, for example, refs 42 and 44.) This is not the case here, since the homogeneous spectral width is substantial compared to the width of $p(\delta)$.

(46) For this deconvolution we used the fast Fourier transform algorithm described in: Press, W. H.; Flannery, B. P.; Teukolsky, S. A.; Vetterling, W. T. *Numerical Recipies*; Cambridge: New York, 1986; Chapter 12.

(47) The harmonic oscillator model we employed is a standard model (see refs 48 and 49) based on treating the upper and lower states of the transition as shifted harmonic wells of the same frequency ω. For a single displaced mode, $g(\nu)$ is given by

$$g(\nu) = \sum_{n=0}^{\infty}\left\{\frac{\Delta^{2n}}{2^n n!}\right\} \exp(-\Delta^2/2)h(\nu - \nu_{00} - n\omega)$$

with $h(\nu)$ the homogeneous line shape (assumed Gaussian). In practice, at least two displaced harmonic modes (with distinct values of ω and Δ) were needed to fit the shapes of the low-temperature absorption spectra studied here.

(48) Lin, S. H. *Theor. Chim. Acta* **1968**, *10*, 301. Lin, S. H.; Colangelo, L. J.; Eyring, H. *Proc. Natl. Acad. Sci. U.S.A.* **1971**, *68*, 2135.

(49) Ballhausen, C. J. *Molecular Electronic Structures of Transition Metal Complexes*; McGraw-Hill: New York, 1979; Chapter 4.

(50) Becker, P. C.; Fragnito, H. L.; Bigot, J. Y.; Brito Cruz, C. H.; Fork, R. L.; Knox, W. H.; Shank, C. V. *Phys. Rev. Lett.* **1989**, *63*, 505. Brito Cruz, C. H.; Fork, R. L.; Knox, W. H.; Shank, C. V. *Chem. Phys. Lett.* **1986**, *132*, 341.

(51) Rosker, M. J.; Wise, F. W.; Tang, C. L. *Phys. Rev. Lett.* **1986**, *57*, 321.

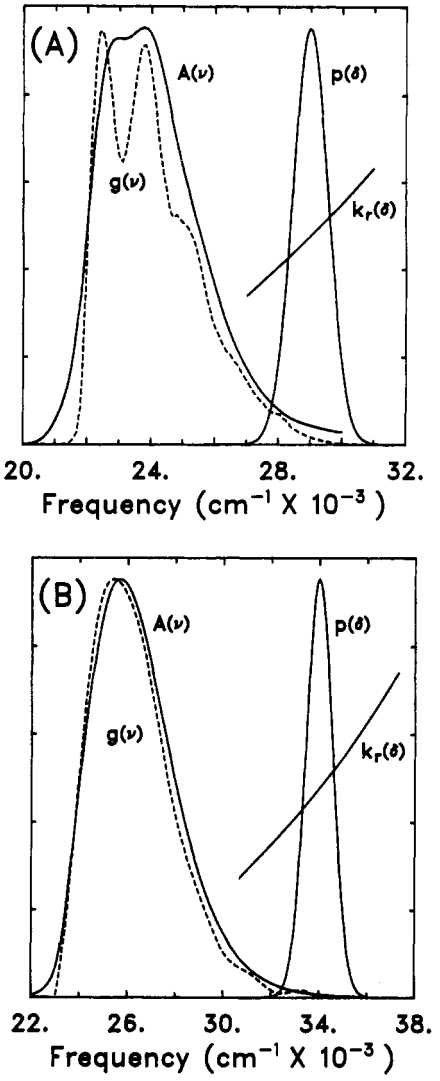

Figure 7. Decomposition of the absorption spectra ($A(\nu)$) of Figures 4 and 5 into $g(\nu)$ and $p(\delta)$ components (see text). The dependence of the radiative rate k_r on δ is also shown superimposed on $p(\delta)$. (A) Cu153 in 1-propanol at 88 K; (B) 4-AP in 1-propanol at 88 K.

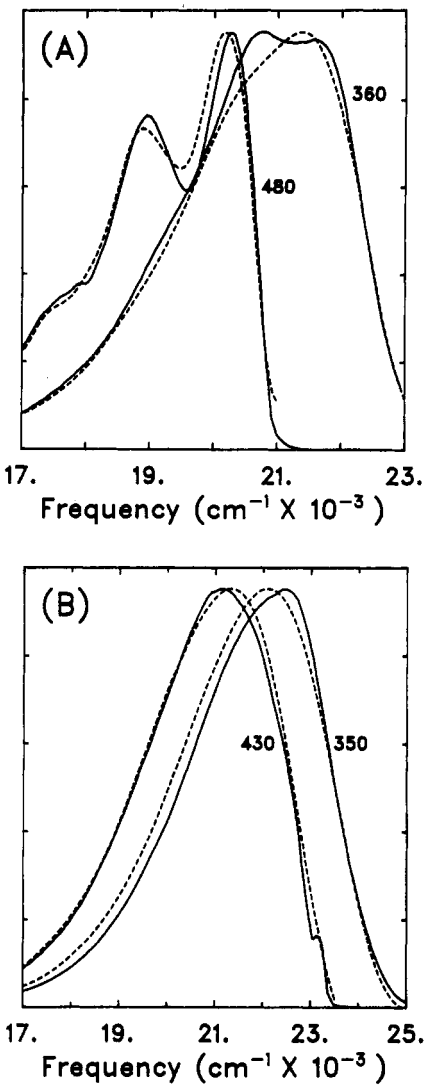

Figure 8. Steady-state fluorescence spectra calculated on the basis of the spectral decompositions of Figure 7. The solid curves are the experimental data and the dashed curves the model predictions. Typical spectra obtained with excitation on the blue and red spectral edges are shown (excitation wavelengths indicated). (A) Cu153 in 1-propanol at 88 K; (B) 4-AP in 1-propanol at 88 K.

of similar fluorophores roughly an order of magnitude larger than this at room temperature, the "homogeneous" widths here probably only reflect underlying substructure to these bands. Also shown on these plots is the variation of k_{rad} with δ, calculated assuming the validity of eqs 9 and 10. According to eq 8 the steady-state spectrum is unaffected by this k_{rad} dependence (for negligible k_{nr}), but it is this dependence that gives rise to the time-dependent spectral shifts.

In addition to reproducing the excitation dependence of the ν_+ frequencies, the inhomogeneous broadening model also accounts for the observed changes in spectral width and shape. Typical results for the systems illustrated in Figures 4 and 5 are shown in Figure 8. Here we have plotted observed and calculated fluorescence spectra for excitation frequencies on the red and blue edges of the absorption bands. The fact that the fluorescence spectra can be well reproduced based on a $g(\nu)$ obtained from absorption data implies that the assumption of mirror symmetry, i.e., nearly equal vibrational spacings in the ground and excited states, is appropriate in these probes. Finally, we note that minor differences between the observed and calculated spectra can be seen in Figure 8. These appear to be due to errors in the $g(\nu)$ determination rather than to any inadequacies in the modeling.

Before discussing the time dependence of the fluorescence spectra, some comments are in order regarding the inhomogeneous widths, Γ_{inh}, determined from these REE experiments. To our knowledge, the results summarized in Table II represent virtually the only direct measurements of the inhomogeneous contribution to the absorption spectra of solvatochromic probes. Although there is a growing literature concerning the homogeneous line widths of similar chromophores in low-temperature organic glasses,[53] workers have not attempted to extract the inhomogeneous contribution to the overall (largely vibronic) width of the absorption spectrum. One exception is an early study by Funfschilling et al.,[42] who determined what we have called $p(\delta)$ for the phosphorescence spectrum of 1-iodonaphthalene in bromobutane at 5 K. These authors observed a Gaussian $p(\delta)$ of width $\Gamma_{inh} = 190$ cm^{-1} for this system. The values obtained in the present study are roughly an order of magnitude larger. The larger widths observed here reflect the much larger coupling of these fluorescence transitions to the solvent than the phosphorescence transitions of 1-iodonaphthalene.

For comparison to the measured inhomogeneous widths, in Table II we also list the fwhm (Γ_{abs}) of the absorption spectrum at 88 K and the difference ($\Delta\Delta\nu$) between the steady-state Stokes shifts ($\nu_{abs} - \nu_{em}$) observed at 298 and 88 K. Assuming no solvent

(52) Chesnoy, J.; Mokhtari, A. *Phys. Rev.* **1988**, *A38*, 3566.

(53) See for example the reviews: Jankowiak, R.; Small, G. R. *Science* **1987**, 237, 618. Volker, S. *Annu. Rev. Phys. Chem.* **1990**, *40*, 499. See also papers by Fayer and co-workers cited in: Littau, K. A.; Bai, Y. S.; Fayer, M. D. *J. Chem. Phys.* **1990**, *92*, 4145.

relaxation at 88 K and relaxation fast compared to k_{fl} at 298 K, the latter quantity measures the total fluorescence shift available from solvent reorganization. As already mentioned, the inhomogeneous contribution to the spectra in these systems is large. In the cases studied, Γ_{inh} is between 25 and 50% of the width of the absorption spectrum. Γ_{inh} is also substantial compared to the fluorescence Stokes shift due to solvent relaxation; Γ_{inh} is between 40 and 100% of $\Delta\Delta\nu$ in these probes and solvents. The largest Γ_{inh} values are such that there is appreciable overlap between the distributions of solvent environments in equilibrium with the S_0 and S_1 states. We note that the relative magnitudes of the inhomogeneous widths show the expected behavior with respect to variations of probe molecule and solvent. Since Γ_{inh} and $\Delta\Delta\nu$ both measure the strength of the coupling between the probe and solvent,[54] one would expect these two parameters to be correlated. With the exception of Cu102 in propanol, the data in Table II show a reasonable correlation between Γ_{inh} and $\Delta\Delta\nu$. Thus, within the series of different probes in propanol we have $\Gamma_{inh}(M1) \approx \Gamma_{inh}(2\text{-AA}) < \Gamma_{inh}(Cu153) < \Gamma_{inh}(4\text{-AP})$ as anticipated from the $\Delta\Delta\nu$ values. Similarly, the larger values of Γ_{inh} for M1 in ethylene glycol + water and for 4-AP in glycerol compared to propanol reflect the larger interactions with these solvents than with propanol, as measured by $\Delta\Delta\nu$.

The one exception to these observations is Cu102 in propanol, whose Γ_{inh} is considerably smaller than would be expected on the basis of the remaining data. Considering their similar chemical structure and comparable $\Delta\Delta\nu$ values, one would anticipate Γ_{inh} for this system to be close to that for Cu153 in propanol, $\Gamma_{inh} \sim 1300\ cm^{-1}$. The value observed for Cu102 in propylene carbonate also suggests such a value, rather than the value of $\Gamma_{inh} = 790\ cm^{-1}$ actually observed. The time-dependent spectral shift observed with this system (see section VI) is also similar to that of the Cu153/propanol system, again suggesting that the inhomogeneous broadening should be similar in the two systems. However, we have repeated measurements on this system several times with similar results. Furthermore, the red edge of the absorption spectrum of Cu102 in propanol is much sharper than the corresponding spectrum of Cu153, in keeping with the reduced value of Γ_{inh}. Thus, the puzzling result for Cu102 in propanol does not appear to be merely an experimental artifact.

Finally, we note that the inhomogeneous solvent distributions determined here do not correspond to equilibrium distributions at the measurement temperatures. All of the systems studied are nonequilibrium glasses. The distributions that we observe actually correspond to those in quasi-equilibrium at higher temperatures, near T_g. During sample cooling there comes a point at which structural relaxation has effectively ceased on the experimental time scale (hours). It is the distribution which is frozen in at this point that we actually observe. The spectra recorded in propanol are reproducible from sample to sample, and thus the distributions we derive from them are well-defined quantities. In glycerol the situation is less satisfactory. Results in this solvent do appear to be influenced by sample preparation, probably due to the fact that glycerol is so viscous at room temperature. The two glycerol data points shown in Table II were recorded with different samples, and the differences between them may reflect more the differences in sample preparation than changes with temperature.

VI. Time-Dependent Shifts

Some of the general characteristics of the fluorescence dynamics observed in frozen solvents are illustrated in Figures 9 and 10. In Figure 9 we show time-resolved data recorded with the probe 4-AP in 1-propanol glass at 88 K. In this system, as in almost all cases studied, the emission at any wavelength can be well represented by a single-exponential decay over the time scale of several fluorescence lifetimes (excluding fluorescence due to small amounts of impurities[55]). However, the rate of decay varies across the fluorescence band, as illustrated in Figure 9A. In this panel we have plotted the fluorescence decay rate at a given frequency, $k_{fl}(\nu)$, normalized to the decay rate of the entire emission band, $k_{fl} = 1/\tau_{fl}$ (Table II). The latter quantity is defined as the rate of decay of total fluorescence integrated over the emission spectrum. This total fluorescence decay is also found to be well represented as a single-exponential function. The variation of fluorescence decay rate with emission frequency gives rise to

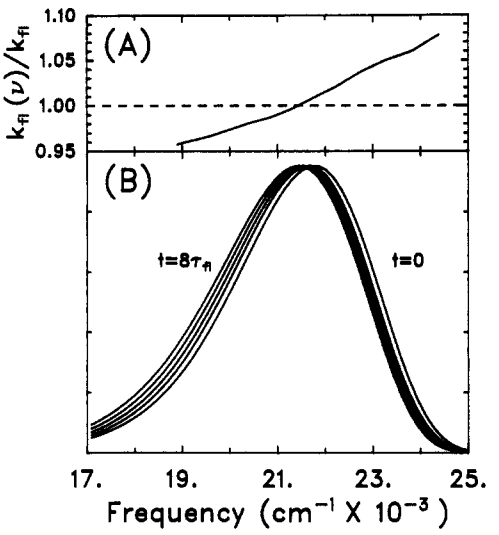

Figure 9. Characteristics of the time-dependent fluorescence observed with 4-AP in 1-propanol at 88 K. (A) Variation of the normalized fluorescence decay rate $k_{fl}(\nu)/k_{fl}$ with emission frequency. In this expression, k_{fl} is the decay rate of the total (integrated) emission. (B) Fluorescence spectra observed at times of 0, 2, 4, 6, and $8\tau_{fl}$. The smooth curves shown here are the fits of the experimental spectra (15 frequencies) to a log-normal line-shape function.

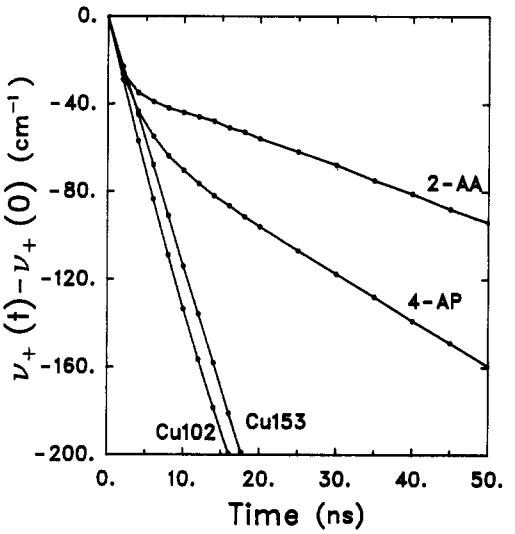

Figure 10. Time dependence of the fluorescence frequency ν_+ for several probes in 1-propanol at ~88 K. Frequencies have been shifted so as to coincide at $t = 0$. The relatively fast decays observed in 2-AA and 4-AP at early times are due to small amounts of impurities in these systems.[55]

(54) Within a linear point dipole model, the fluorescence Stokes shift due to solvation (i.e., the quantity measured by $\Delta\Delta\nu$) is proportional to $\mu_e(\mu_e - \mu_g)\pi$ whereas the width of the absorption or emission spectrum is proportional to $(\mu_e - \mu_g)^2\pi$. In these expressions μ_g and μ_e are the ground- and excited-state dipole moments of the probe, assumed collinear (see ref 27), and π is some sort of solvent polarity measure.

(55) In both 4-AP and 2-AA in propanol at 88 K we observed decay components on the blue side of the probe fluorescence having lifetimes of ~3–5 ns. The integrated intensity of these components was less than 1% of the total fluorescence intensity, and no obvious signs of their presence were observed in the steady-state fluorescence spectra. Attempts at further purification of the probes and the solvent did not substantially alter the amount of this emission, and its origin is at present uncertain. Based on the spectra and decay times of the protonated species ($-NH_3^+$), a small concentration of protonated molecules at low temperatures appears to be a possible explanation. In any case, the lifetimes of the probes (~20 ns) are sufficiently distinct from the decay times of the impurity fluorescence so as to make the two easily separable. In reporting the slopes $d\nu/dt$ in Table II we have ignored the short-time behavior.

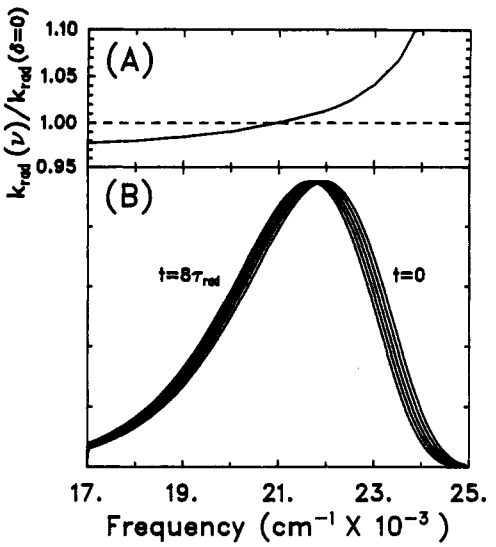

Figure 11. Characteristics of the time-dependent fluorescence calculated on the basis of the inhomogeneous kinetic model and corresponding to the experimental data of Figure 9: (A) variation of the normalized fluorescence decay rate $k_{rad}(\nu)/k(\delta=0)$ with emission frequency; (B) fluorescence spectra observed at times of 0, 2, 4, 6, and $8\tau_{rad}$.

time-evolving spectra of the sort shown in panel b of Figure 9. In order to smooth out noise in the experimental data, we typically fit observed spectra (Figure 1) to a log-normal line-shape function.[8,56] The curves in Figure 9B are such log-normal fits to the (15-point) experimental data at times of 0, 2, 4, 6, and $8\tau_{fl}$. Note that the width and shape of the spectrum are not changing noticeably in time.

To monitor the dynamics of time-evolving spectra such as these, we again utilize the high-frequency half-maximum point, $\nu_+(t)$. Figure 10 summarizes results for four different probe solutes in propanol glass ($T \sim 88$ K). For convenience we have shifted all frequencies so as to coincide at $t = 0$. Two features of these curves deserve comment. First, as mentioned in section III, the spectra of different probes shift at very different rates in a single solvent. This behavior would be difficult to rationalize in terms of solvent dynamics, given that all of these probes behave similarly at higher temperatures. Within the inhomogeneous decay model, such differences are easily explained in terms of the different fluorescence lifetimes of the various probes (τ_{fl}, Table II). It is the latter (or more precisely the radiative component of τ_{fl}) which sets the time scale of the inhomogeneous spectral shift. That is, all of the decays are similar if viewed on a time axis normalized to their respective lifetimes (see Figure 12). The second feature typical of these shifts is that over the available time window they are approximately linear functions of time. (In making this observation we are ignoring the early-time behavior of the probes 4-AP and 2-AA, which is due to the presence of small amounts of fluorescent impurities in these samples.[55] The approximate linearity of the $\nu_+(t)$ plots allows for a simple characterization of the dynamics in terms of the slopes, $d\nu_+/dt$, which are listed in Table II.

We now compare the observed time dependence with that predicted on the basis of the inhomogeneous kinetic model of section IV. We use the $g(\nu)$ and $p(\delta)$ functions determined from the analysis of red-edge excitation experiments described previously. With the exception of the assumed models for k_{rad} and k_{nr} (eqs 9 and 10), calculation of the time-dependent fluorescence entails no further assumptions or adjustable parameters.

Figure 11 shows the calculated spectral dynamics of the 4-AP/1-propanol (88 K) system, which is to be compared to the experimental results of Figure 9. The same features observed in the experiments are reproduced in the calculated dynamics. At any emission wavelength, the fluorescence decay ($F(t)$, eq 6) is calculated to be a single-exponential function. Thus, even though the decay at any wavelength consists of a superposition of distinct radiative rates ($k_{rad}(\delta)$, Figure 7B), the spread in rates is not large enough to cause significant departure from exponentiality on the time scale of 0–6 fluorescence lifetimes. Comparison of Figures 9A and 11A shows that the simulations reproduce the systematic variation of decay rate as a function of frequency. Although the agreement is not perfect, the general trend as well as the magnitude of the variation in rates is accounted for. Note that in making the above comparison, in addition to our assumption that all of the solvent dependence of k comes from k_{rad}, we further assume that $k_{nr} = 0$. The fact that the calculated $k_{rad}(\nu)/k_{rad}(\delta=0)$ and the observed $k_{fl}(\nu)/k_{fl}$ functions are in essential agreement justifies this neglect of k_{nr}. Comparing Figures 11B and 9B also shows that the calculated spectral evolution also reproduces the experimentally observed behavior. As is the case experimentally, the calculated fluorescence spectra shift in time without undergoing any noticeable narrowing or change in shape. This aspect of the dynamics is perhaps not intuitive. One might have instead anticipated that an inhomogeneous decay mechanism would lead to a narrowing of the spectrum due to preferential depletion of the blue spectral edge. That this does not occur is a result of the nature of the $k(\delta)$ dependence used here.[57]

The final comparison to be made between the observed dynamics and model calculations is with the $\nu_+(t)$ curves, several of which are shown in Figure 12. In addition to the results for the 4-AP/propanol system considered in Figures 9 and 11, we also show the results for three other representative cases. These data have been scaled by the respective fluorescence lifetimes in order to show the similarity of the behavior of different probes.[58] The calculated $\nu_+(t)$ curves are linear functions of time over the available range, as are the experimental data. The agreement between the observed and calculated curves is reasonable, although not quantitative in all instances. The largest relative deviation from the observed shifts is observed for the Cu102/propanol system (curve a). The difference between the calculated and observed slopes in this case is greater than a factor of 2, a much larger deviation than found for the remaining systems studied. This poor agreement with the calculations can be traced to the unexpectedly small value of Γ_{inh} estimated for this system.

A more complete comparison between the observed and calculated dynamics can be obtained from the scaled slopes, $(1/k_{fl})(d\nu_+/dt)$, which are summarized in Table II and plotted in Figure 13. With the exception of Cu102 in propanol, the calculated slopes are within ±50% of those observed. Although there is considerable scatter in the data, no systematic deviations from the inhomogeneous kinetic predictions are apparent from Figure 13. Since the calculations were performed with no adjustment of parameters subsequent to the red-edge analysis, we consider the agreement shown here to be satisfactory. The model calculations display the correct qualitative behavior and furthermore provide a semiquantitative account of the observed time dependence. On the basis of such agreement we conclude that the apparent "relaxation" observed at low temperatures is in fact due to nondynamical, inhomogeneous kinetics of the sort described above.

(56) Siano, D. B.; Metzler, D. E. *J. Chem. Phys.* **1969**, *51*, 1856.

(57) Spectral narrowing requires that the excited-state distribution $p_e(\delta)$ narrow substantially in time. That this does not happen in the present case is due to the fact that $p_e(\delta)$ is a continuous function of δ and in addition that the change of $k(\delta)$ over the width of this distribution is relatively modest. Under such conditions, $p_e(\delta)$ shifts in time without any noticeable change in width. Relaxing either of these two conditions would lead to spectral narrowing observable on the time scale of several fluorescence lifetimes. For example, in ref 7 Agmon develops a two-state model of inhomogeneous decay kinetics. In this discontinuous $p(\delta)$ model the spectrum narrows in time as a two-site mixture is transformed into a single-component system and the spectrum asymptotically approaches that particular shift and width appropriate to the final state of the solvent distribution. For a continuous $p(\delta)$, the distribution does not approach any asymptotic limit; however, its width can still change as long as $k(\delta)$ varies rapidly enough with δ.

(58) Due to the assumption that k_{nr} is independent of solvent site, the time-dependent shifts calculated from the model scale with k_{rad}; i.e., $\nu_+ = \nu_+(k_{rad}t)$. In comparing these calculated dependences with experimental observations scaled according to k_{fl}, we are again assuming that k_{nr} is negligible compared to k_{rad} at the low temperatures studied.

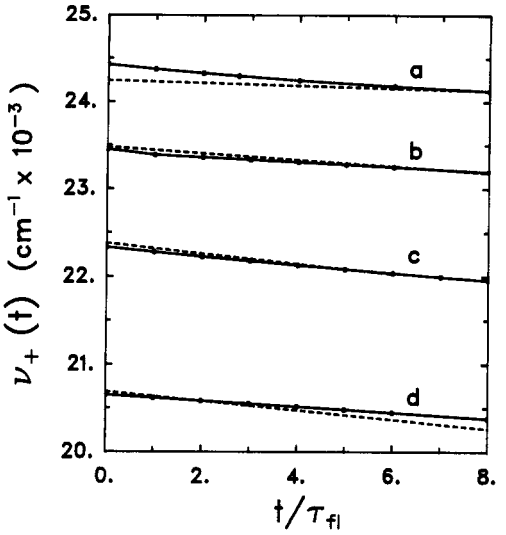

Figure 12. Comparison of observed (solid) and calculated time-dependent shifts for several representative systems. All temperatures are ~88 K (see Table II), and the solvent is 1-propanol unless otherwise noted. The systems shown are (a) Cu102, (b) 4-AP, (c) Cu153, and (d) M1 in a 4:1 ethylene glycol/water mixture. The time axis has been scaled with respect to the fluorescence lifetime in the case of the experimental data and with respect to the radiative lifetime ($1/k_{rad}(\delta=0)$) in the case of the calculations. In comparing these data, we are assuming that $k_{nr} \ll k_{rad}$.

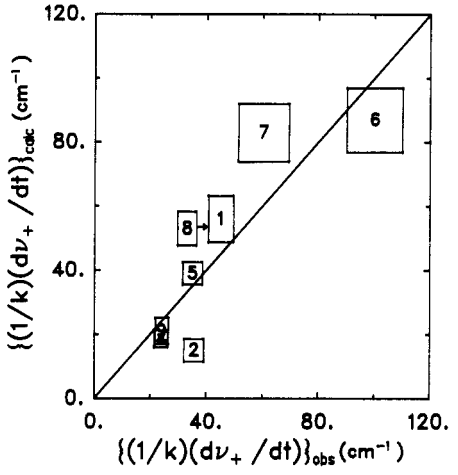

Figure 13. Comparison of observed and calculated slopes $(1/k)(d\nu/dt)$. Numbers correspond to those provided in Table II, and the boxes enclosing the data points represent estimated uncertainties. The slopes have been scaled by $1/k_{rad}(\delta=0)$ in the case of the calculations and $1/k_{fl}$ in the case of the experimental data. These two scale factors are the same under the assumption that $k_{rad} \gg k_{nr}$. With the possible exception of the M1 probe (no. 8), this condition should be well satisfied for the probes studied. In the latter case, relaxing this assumption would lead to a change in the observed value in the direction indicated by the arrow.

VII. Summary and Conclusions

We have observed time-dependent shifts in the fluorescence spectra of solvatochromic probe molecules in frozen polar solvents. The phenomenon is a general one and is observed in a variety of fluorophores in both hydrogen-bonding and non-hydrogen-bonding solvents. Since the shifts are observed at temperatures where no solvent relaxation is expected, their origin does not lie in the same dynamical mechanism widely studied under fluid conditions. Rather, time-dependent shifts in frozen solvents can be understood as resulting from inhomogeneous fluorescence decay kinetics. Molecules in different portions of the fluorescence spectrum decay at different rates and thereby cause the spectrum to evolve in time due to a nonuniform loss of excited-state population.

Two requirements must be met for this type of mechanism to operate. The first is the presence of a distribution of solvent environments that gives rise to an inhomogeneous distribution of solvent-induced spectral shifts. This condition is readily fulfilled with common solvatochromic probes, as indicated by the fact that they all show substantial excitation-dependent emission shifts (i.e., the REE effect) in frozen polar solvents. The second requirement is that the fluorescence decay rates of molecules in different solvent environments be correlated with their emission frequencies. Such a correlation between frequency and decay rate is provided by the universal dependence of k_{rad} on ν^3.

In the present study, we have used a simple spectral model to analyze red-edge excitation experiments in order to characterize the inhomogeneous broadening present in a number of fluorophore/solvent systems. With the further assumption that the fluorescence lifetime is solvent sensitive only via the relation $k_{rad} \propto \nu^3$, we could also calculate the time dependence of the fluorescence spectra. Such calculations are able to semiquantitatively reproduce the time dependence observed at low temperatures. With the exception of the Cu102/1-propanol system, the rate of spectral shift ($d\nu/dt$, Table II) calculated is within 50% of the observed value. We interpret this semiquantitative agreement as an indication that the overall picture of inhomogeneous decay kinetics described here is essentially correct. Any deviations from the model predictions can be reasonably ascribed to the assumption that the solvent effect on emission rates enters only via the ν^3 relation. It would not be surprising to find that additional mechanisms also contribute to the variation of the fluorescence decay rate with solvent shift. For example, one might expect both k_{rad} and k_{nr} to vary slightly with δ as a result of solvent-induced changes in the electronic wave function of the solute. Such additional solvent influence would modify the observed dynamics and might well account for the deviations from the behavior predicted, as for example, in the case of Cu102 in propanol.

Kim and Hynes[59] have recently made significant progress toward understanding these other sorts of solvent effects on the fluorescence of polar solutes. They have used a two-state solute model involving mixing between a nonpolar ground state and a charge-transfer excited state to study how the electronic properties of highly polar excited states are modified by solvation. Within the context of this model, Kim and Hynes predict that the transition moment for emission varies with solvation state in such a way that the radiative rate follows a ν^α type law. Possible values of α range between $\alpha = 1$ and $\alpha = 3$ depending on the relative orientation of the permanent and transition dipole moments of the probe. (Parallel moments are predicted to produce a value 1 while perpendicular moments yield the value 3.) In addition to the calculations described above, we have also applied the other limiting frequency dependence predicted by this model, $k_{rad} \propto \nu^1$. We find that the cases studied here are better described as being near the $\alpha = 3$ limit. As already mentioned, when the solvent dependence of k_{rad} of Cu102 (Figure 3) is fit to a power law $(k_{rad}/n^3) \propto \nu^\alpha$, we observe $2 \leq \alpha \leq 3$. Similarly, the agreement between the observed time-dependent shifts and those calculated as described above (Table II) is much better with the choice $k_{rad} \propto \nu^3$ than with $k_{rad} \propto \nu^1$. With the latter choice, the slopes $(d\nu_+/dt)$ tend to be much smaller than experimentally observed. It is unclear at present why the $\alpha = 3$ (perpendicular) limit should apply to the molecules used here, and more study is needed to understand the solvent dependence of k_{rad} more fully. Such studies may, in time, allow for a more quantitative description of the low-temperature shifts than has been possible here. However, the general findings of the present study should not be significantly altered by the outcome of such further investigation.

In closing, it is useful to consider the implications of our findings in relation to studies of solvation dynamics. First, they clearly point to the need for caution when interpreting low-temperature time-dependent fluorescence shifts in terms of solvent relaxation. Especially when observations are made on time scales comparable to or longer than the probe lifetime, inhomogeneous decay kinetics will significantly influence the spectral dynamics. Neglecting this effect will lead to erroneous conclusions concerning the solvent dynamics. Thus, while the fluorescence spectra of many probe

(59) Kim, H. J.; Hynes, J. T. Preprint.

molecules exhibit time-dependent shifts in propanol glass at 88 K, our analysis shows that it is unlikely that significant solvent relaxation processes occur in this system on the nanosecond time scale.

Fortunately, review of the existing literature on solvation dynamics shows that few previous studies are likely to have been incorrectly interpreted on this account. With the exception of very early studies by Ware and co-workers,[14,60] most experiments have been limited to temperatures for which the spectral shift was observed to take place within the fluorescence lifetime of the probe. The effect of inhomogeneous decay kinetics should be negligible in such cases. Even for the most extreme example studied here, 4-AP in glycerol, the shift due to this mechanism is only ~70 cm^{-1} during one probe lifetime. This shift amounts to a mere 2% of the ~3500-cm^{-1} change (Table II) expected to result from solvent reorganization in this system. In making the above judgement, we have used results based on behavior observed in frozen solvents to estimate the influence of inhomogeneous kinetics at higher temperatures where the solvent is fluid. Two opposing factors will modify the actual effect of solvent inhomogeneities expected in fluid compared to rigid solvents. First, the extent of inhomogeneous broadening of the absorption spectrum should increase (approximately as $T^{-1/2}$ [4,28,30]). This change will serve to increase the influence that inhomogeneous decay kinetics have on the spectrum. However, if the average solvation energy (or spectral shift) changes with time, so too will the distribution over solvent sites. Such "spectral diffusion" among different components of the excited state $p_e(\delta)$ distribution is predicted to occur at a rate twice that of the average frequency shift.[4,29] This aspect of the fluid regime will serve to reduce the effect of the inhomogeneous decay kinetics on the spectral shift, just as it reduces and finally nullifies the REE effect. Although we have not fully modeled this fluid regime,[61] it is clear that inhomogeneous kinetic effects will not be significantly greater under fluid conditions than in frozen solvents. Thus, contrary to the suggestion of Agmon,[7] we find that the influence of spectral inhomogeneity on measurements of average solvation dynamics at high temperatures should be of negligible importance.

We note that similar conclusions were also reached by Wagener and Richert in a recent study of phosphorescent probes in supercooled liquids.[62] In fact, these authors found no evidence for spectral dynamics due to solvent inhomogeneity in most phosphorescent probes, even under frozen solvent conditions. This result may seem surprising since the same effects discussed here should be operative in phosphorescence probes as well. However, the solvent-induced spectral shifts in the former molecules are roughly 10 times smaller than in commonly employed fluorescence probes. The effect of solvent inhomogeneity on the phosphorescence decay rates is thus apparently reduced to unobservably small levels in such cases.[63]

Acknowledgment. We thank Ranko Richert and Casey Hynes for communication of their results prior to publication and Noam Agmon for many interesting discussions on the subject of inhomogeneous kinetics. Acknowledgment is made to the donors of the Petroleum Research Fund, administered by the American Chemical Society, and the Division of Chemical Sciences, Office of Energy Research, U.S. Department of Energy, for support of this work.

(60) Chakrabarti, S. K.; Ware, W. R. *J. Chem. Phys.* **1971**, *55*, 5494.

(61) Reference 4 does describe such a theory for the case where the spectral shift due to solvent relaxation is a single-exponential function. Unfortunately, the solvation dynamics in these liquids is far from single exponential and a considerably more sophisticated theory is required for their treatment.

(62) Wagener, A.; Richert, R. *Chem. Phys. Lett.* **1991**, *176*, 329. See also: Richert, R. *Ibid.* **1990**, *171*, 222.

(63) Wagener and Richert did not observe inhomogeneous decay kinetics due to the sort of solvent effects discussed here. They did, however, observe such kinetics in the presence of heavy atoms (Br) which influence k_{nr} in some of their phosphorescent probes.

MNDO-PM3 Calculations of Activation Energies for the Addition of Chlorinated C_1 and C_2 Radicals to Chlorinated Ethylenes and Acetylenes

Yun Shi and Selim M. Senkan*

Department of Chemical Engineering, University of California, Los Angeles, California 90024
(Received: December 5, 1990)

Activation energies for the addition of chlorinated C_1 and C_2 (vinylic) hydrocarbon radicals to similarly chlorinated ethylenes and acetylenes were studied theoretically by using the semiempirical MNDO method and the PM3 set of parameters at the UHF level. Calculated activation energies increased with increasing chlorine substitution of the species, and β sites were determined to be the preferred addition sites. The results also correlated with Evans-Polanyi relationships.

Introduction

The addition of chlorinated C_1 and C_2 radicals to unsaturated hydrocarbons and chlorinated hydrocarbons (CHC) is important in hazardous waste incineration[1] as well as in industrial chemistry. Such addition reactions are responsible for molecular weight growth in the gas phase, which subsequently can result in the production of potentially toxic chlorinated aromatic hydrocarbons, such as chlorinated phenols, polychlorinated dibenzodioxins (PCDD), and dibenzofurans (PCDF).[2] Further increase in molecular weight ultimately leads to the production of tars, soot, and coke which are also undesirable byproducts.[3-6]

Although considerable data exist on the addition of C_1 and C_2 hydrocarbon radicals to C_2H_4 and C_2H_2, both as a result of experimental[7] and theoretical[8-10] investigations, similar information

* To whom correspondence should be addressed.

(1) Senkan, S. M. *Environ. Sci. Technol.* **1988**, *22*, 368.
(2) Altwicker, E. A.; Schonberg, J. S.; Konduri, R. K. N. V.; Milligan, M. S. *J. Hazard Waste Hazard. Mater.* **1990**, *7*, 73.
(3) Robinson, J. M.; Gupta, A. K.; Senkan, S. M. *Combust. Flame* **1983**, *49*, 305.
(4) Weissman, M.; Benson, S. W. *Prog. Energy Combust. Sci.* **1989**, *15*, 273.
(5) McKinnon, J. T.; Howard, J. B. *Combust. Sci. Technol.*, in press.
(6) Frenklach, M. *Combust. Sci. Technol.*, in press.
(7) Kerr, A. J.; Moss, S. J. *Handbook of Bimolecular and Termolecular Gas Reactions*; CRC Press: Boca Raton, FL, 1980; Vol. II.

0022-3654/91/2095-5181$02.50/0